



Conformational rearrangements in the N-domain of *Escherichia coli* FepA during ferric enterobactin transport

Received for publication, November 26, 2019, and in revised form, February 14, 2020. Published, Papers in Press, February 25, 2020, DOI 10.1074/jbc.RA119.011850

Aritri Majumdar[‡], Vy Trinh[§], Kyle J. Moore[¶],  Chuck R. Smallwood^{||}, Ashish Kumar[‡], Taihao Yang[‡], Daniel C. Scott^{**}, Noah J. Long[‡],  Salet M. Newton[‡], and Phillip E. Klebba^{‡1}

From the [‡]Department of Biochemistry and Molecular Biophysics, Kansas State University, Manhattan, Kansas 66506, the [§]Department of Chemistry and Biochemistry, University of Oklahoma, Norman, Oklahoma 73019, the [¶]Department of Chemistry, Physics and Engineering, Cameron University, Lawton, Oklahoma 73505, the ^{||}Sandia National Laboratories, Albuquerque, New Mexico 87185, and the ^{**}Howard Hughes Medical Institute, St. Jude Children's Research Hospital, Memphis, Tennessee 38105

Edited by Chris Whitfield

The *Escherichia coli* outer membrane receptor FepA transports ferric enterobactin (FeEnt) by an energy- and TonB-dependent, but otherwise a mechanistically undetermined process involving its internal 150-residue N-terminal globular domain (N-domain). We genetically introduced pairs of Cys residues in different regions of the FepA tertiary structure, with the potential to form disulfide bonds. These included Cys pairs on adjacent β -strands of the N-domain (intra-N) and Cys pairs that bridged the external surface of the N-domain to the interior of the C-terminal transmembrane β -barrel (inter-N–C). We characterized FeEnt uptake by these mutants with siderophore nutrition tests, [⁵⁹Fe]Ent binding and uptake experiments, and fluorescence decoy sensor assays. The three methods consistently showed that the intra-N disulfide bonds, which restrict conformational motion within the N-domain, prevented FeEnt uptake, whereas most inter-N–C disulfide bonds did not prevent FeEnt uptake. These outcomes indicate that conformational rearrangements must occur in the N terminus of FepA during FeEnt transport. They also argue against disengagement of the N-domain out of the channel as a rigid body and suggest instead that it remains within the transmembrane pore as FeEnt enters the periplasm.

The crystal structures of some Gram-negative bacterial outer membrane (OM)² proteins clarified or rationalized their functionalities. For instance, the crystal structures of general porins (1, 2) showed open trans-OM channels, with a 10 Å constriction zone that explained the size-exclusion properties of the pore. These data revealed why OmpF and its relatives exclude large

molecules but allow passage of small (< ~600 Da) hydrophilic solutes, as was previously defined (3, 4). Similarly, the structure of the maltoporin, LamB (5), revealed a narrower (~6 Å diameter) open pore decorated on the exterior and within the pore constriction zone by aromatic residues, that explained its selectivity for maltodextrins (6, 7). The situation was different for OM siderophore receptors like FepA and its relatives. Aside from revealing 22 stranded β -barrels topped with large loops that form a cell-surface vestibule for ligand binding, their crystal structures (8–12) did not explain their transport mechanisms and posed the quandary of transmembrane channels obstructed by ~20-kDa globular domains. Instead of revealing an obvious path for ligand uptake, the structures implied that conformational changes must occur to allow internalization of bound ligands. The energy and TonB dependence (13) of OM iron transport rationalized these predicted protein dynamics. Despite this insight, the structural changes that facilitate ligand uptake through TonB-dependent transporters (14) are not yet understood. Such OM proteins are not typical transporters, a term that usually refers to ATP- or protonmotive force-driven inner membrane permeases (15). Another designation for OM siderophore receptors in this superfamily (16, 17) is ligand-gated porin (LGP) (18), which alludes to the fact that ligand binding initiates their uptake reaction and calls to mind their transmembrane porin β -barrels. However, LGPs are not diffusive porins. Unlike OmpF (3, 19) or LamB (20), LGPs like FepA (8) do not contain open transmembrane pores. Rather, energy-dependent uptake through their closed channels (a globular N terminus situated within a C-terminal β -barrel) is regulated by TonB action (13). This report focuses on conformational rearrangements within LGP that allow internalization of bound ligands.

Many different LGPs across many families of Gram-negative bacteria transport ferric siderophores, heme, other metal complexes (21) and other small molecules (e.g. sugars in *Caulobacter crescentus* (22–24)). Iron acquisition systems are virulence determinants (25) of bacterial pathogens that secrete siderophores to scavenge iron or hemophores to strip heme from host-binding proteins (26). Hence, explication of the molecular mechanism of OM iron uptake may lead to new approaches or new compounds against bacterial pathogens (27). LGPs bind ligands in their surface vestibules by induced fit (28, 29), creating sub-nanomolar affinities at binding equilibrium (28, 30–33)

This work was supported by National Science Foundation Grant MCB09522999 and National Institutes of Health Grants GM53836 and AI115187. The authors declare that they have no conflicts of interest with the contents of this article. The content is solely the responsibility of the authors and does not necessarily represent the official views of the National Institutes of Health.

This work is dedicated to the memories of Dr. Aritri Majumdar and Distinguished Professor H. Ronald Kaback.

This article contains Figs. S1 and S2.

¹ To whom correspondence should be addressed: Dept. of Biochemistry and Molecular Biophysics, 141 Chalmers Hall, Kansas State University, Manhattan, KS 66506. Tel.: 785-532-6268; E-mail: peklebba@ksu.edu.

² The abbreviations used are: OM, outer membrane; β ME, β -mercaptoethanol; FeEnt, ferric enterobactin; Ent, enterobactin; FD, fluorescent decoy; LGP, ligand-gated porin; FM, fluorescein maleimide; NC, nitrocellulose.

and triggering internal protein dynamics that result in signal transduction to TonB in the bacterial periplasm (11, 12, 34, 35). Previous studies concluded that the 150-residue N-terminal globular domain (N-domain) likely exits the C-domain channel into the periplasm during ligand uptake (29, 36, 37). However, these results did not address how the N-domain moves or changes in structure to promote passage of metal complexes or other molecules (38, 39) through the transmembrane pore. The N-domain contains a four-stranded β -sheet, short turns of α -helix, and loops that project into the surface vestibule (Fig. 1A). Hypothetically, the N termini of LGP may allow metal transport by rearranging within the β -barrel to create a pore or by dislodging from the β -barrel, either as a folded domain or by unfolding. During FeEnt uptake through *Escherichia coli* FepA, substitution G54C, on the surface of the N-domain globule, became accessible to alkylation by extrinsic fluorescein maleimide (FM) (37)). This TonB-dependent fluoresceination of G54C did not occur in the absence of FeEnt transport, and the labeling originated from the presence of FM in the periplasm. We concluded from these data that during iron transport the actions of TonBExbBD promoted full or partial exit of the N-domain out of the β -barrel into the periplasmic space.

Herein, we genetically engineered Cys substitutions in *fepA*, encoding pairs of sulfhydryls in presumably close enough proximity to form disulfide bonds, either exclusively within the N-domain (intra-N) of FepA or between its N- and C-domains (inter-N-C) (Fig. 1). If N-domain unfolding or rearrangement occurs during ligand uptake, then we expected intra-N Cys pairs to impair or abrogate FeEnt transport. Conversely, if the N-domain exits the barrel as a folded unit, then disulfide bonds within it may not prevent ligand uptake, but inter-N-C disulfides that hold the N-domain within the β -barrel will inhibit FeEnt uptake. The experiments found that intra-N disulfide bonds prevented FeEnt transport, but the majority of inter-N-C disulfides did not impair iron uptake. These findings indicate that the N terminus of FepA must rearrange during FeEnt uptake, does not exit the channel as a rigid body, and may instead remain within the pore as it allows or promotes passage of FeEnt into the periplasm.

Results

Formation of disulfide bonds in site-directed Cys pair substitution mutants

We analyzed six pairs of Cys substitutions in adjacent β -strands or other parts of the N-domain and nine Cys pairs in regions that potentially bridged the N-domain and β -barrel (Fig. 1) of otherwise WT *fepA* (all carried on pITS23 (40)). For both types of Cys-pair mutants, disulfide bond formation may retard or abrogate FeEnt transport by interfering with conformational dynamics or motions that involve the N-domain of FepA. We selected the locations for the Cys mutations based on their expected proximity to each other in the FepA tertiary structure (Fig. 1). Analysis of the mutant proteins in nonreducing SDS-PAGE (*i.e.* in the absence of β -mercaptoethanol (β ME)), visualized by anti-FepA immunoblots developed with 125 I-protein A, allowed quantification of their expression and

often showed the extent of disulfide bond formation. However, SDS-PAGE/immunoblot analyses did not always reveal the presence of disulfides in FepA. Some Cys pairs (33–120, 42–162, 56–73, and 149–180; Fig. 2A) showed no evidence of disulfide bond formation in the gels or immunoblots; *i.e.* the electrophoretic mobility of those double-Cys derivatives exactly matched that of WT FepA, despite the fact that other experiments showed that they were disulfide-bonded. For many Cys pairs, however, we saw anti-FepA-reactive band(s) with different electrophoretic mobilities than WT FepA (14–300, 27–126, 51–608, 54–585, 77–511, 84–142, 125–141, 128,463, 138–427, and 138–445; Fig. 2A), verifying the presence of disulfide bonds. Nevertheless, disulfide formation appeared incomplete for all but one of these double-Cys constructs: only mutant I14C-G300C produced a homogeneous band with different mobility than that of FepA (Fig. 2A).

The partial disulfide bonding suggested that a fraction of the engineered Cys side chains remained native and unoxidized. To estimate the amount of unreacted Cys sulfhydryls in the mutant proteins, we exposed SDS-denatured cell-envelope fractions from the Cys-pair mutants to FM (5 μ M; 5 min), before and after reduction by 10 mM β ME. Cys side chains in stable disulfide bonds do not react with the extrinsic fluorophore (*e.g.* Cys-487–Cys-494 in WT FepA (41); Fig. S1A). Fluorescent images of the gels (Fig. S1, A and B), standardized by expression levels gleaned from the immunoblots (Fig. S1, C and D) and quantified by image analysis (Fig. S1E), indicated different extents of disulfide formation among the mutants. Prior to reduction, the six intra-N Cys-pair proteins showed variable reactivity with FM (Fig. S1, A and E), showing different extents of disulfide bond formation. Some (27–126 and 125–141) were only slightly modified by FM, suggesting that they were predominantly disulfide-bonded. Others (14–300, 33–120, 56–73, and 84–142) were more reactive and less disulfide-bonded. 44–111 was the most reactive and the least disulfide-bonded. Unlike other intra-N Cys pairs, it was quantitatively modified by FM before exposure to β ME, implying that it did not significantly form a disulfide bond *in vivo*. 14–300, which appeared fully disulfide-bonded in SDS-PAGE/immunoblots (Fig. 2A), was still partially labeled by FM. After reduction by β ME, all the intra-N Cys-pair proteins were better labeled by FM. WT FepA (two Cys) behaved as anticipated: without reduction it was not labeled; after reduction it was labeled to approximately half the level of 44–111 (four Cys). Overall, from observations of the different electrophoretic mobilities of the Cys-pair mutant proteins, and the reactivity of their sulfhydryls to FM, we obtained evidence of their disulfide-bond formation *in vivo*. The experiments revealed that some disulfide bonds (*e.g.* 33–120 and 56–73) did not alter FepA's mobility in SDS-PAGE, that each mutant protein was unique, and that whether particular Cys pairs formed bonds was unpredictable *a priori*. For example, from its position in the crystal structure of FepA, we expected 44–111 to form a disulfide bond, but apparently it did not.

As seen for intra-N Cys pairs, gels and immunoblots of inter-N-C Cys pairs showed partial disulfide-bond formation. Although the 14–300 disulfide appeared complete, a fraction of these mutant proteins was still modified by FM (Fig. S1, A and E), indicating the presence of free sulfhydryls. Partial disulfide

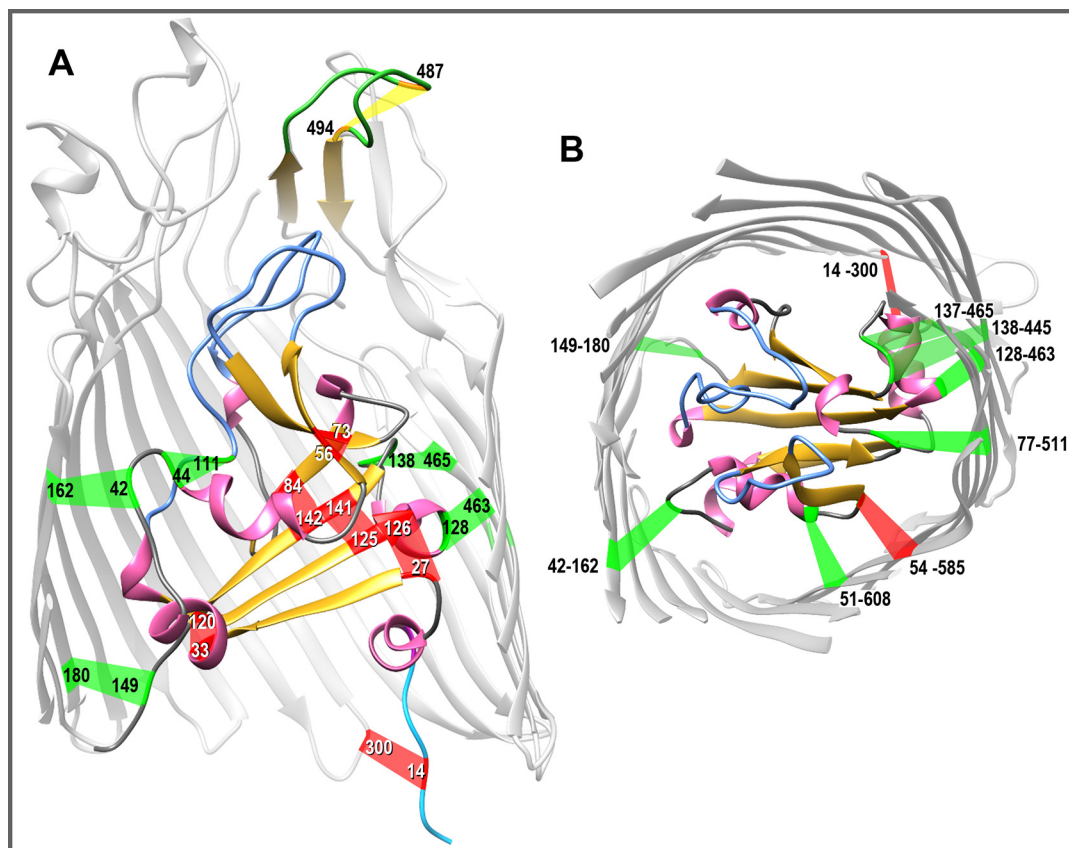


Figure 1. Native and engineered Cys pairs in FepA. From the crystal structure of FepA (1FEP (8)), we modeled the polypeptide (using the Modeller function of CHIMERA) to contain 15 novel Cys pairs, in addition to the native Cys-487–Cys-494 disulfide in L7 of FepA that is resistant to modification unless reduced (46). *A*, side view of Cys pairs. The structure of FepA encompasses a 150-residue globular N-domain within a 574-residue C-terminal β -barrel (only partially rendered to allow a better view of the N-domain). With few exceptions, FepA orthologs contain a natural Cys pair (residues 487–494 in *E. coli* FepA) in L7 (yellow). The flexibility of L7 prevented its delineation in 1FEP (8), but Modeller predicted its disposition. We engineered six individual Cys pairs within the internal globular domain: 27–126, 33–120, 44–111, 56–73, 84–142, and 125–141. We also constructed nine Cys pairs that conjoin the surface of the N-domain and the interior of the β -barrel: 14–300 (37), 42–162, 51–608, 54–585, 77–511, 128–463, 137–465, 138–445, and 149–180. *B*, top view of Cys pairs. We hid the surface loops in the model shown in *A* and rotated it 90° on the *x* axis to reveal the interior of the channel. In both panels, α -helices are pink; β -strands are gold; N-domain loops are blue; and putative disulfide bonds formed by the Cys pairs are colored red if they inhibited FeEnt uptake or green if they did not inhibit FeEnt uptake, as described in the text. The images were rendered from PDB code 1FEP (8) by CHIMERA (UCSF).

formation also occurred between sites 51–608, 54–585, 77–511, 128–463, and 137–465 (Fig. 2A). We did not observe any immunoreactive bands with altered mobility for Cys pairs 42–162 and 149–180.

Effect of engineered Cys pairs on FeEnt utilization in nutrition tests

FeEnt nutrition tests (42) in the absence or presence of β ME showed that the intra-N bonds impaired FepA-mediated transport (Fig. 2D, Fig. S2, and Table 1). In every case that we observed disulfide formation by intra-N Cys pairs, we also observed inhibition of FeEnt uptake through FepA. In the absence of any reducing agent, Cys pairs 27–126, 33–120, 56–73, 84–142, and 125–141 produced 2–3-fold larger and often fainter halos than that of WT FepA (Fig. 2 and Fig. S2). These differences reflected a lower FeEnt uptake rate (43, 44) that was overcome by the inclusion of 1 mM β ME in the test plate. None of the individual Cys substitutions comprising the Cys pairs that we tested impaired FeEnt utilization (Fig. S2). The inhibitory Cys pairs all linked adjacent β -strands in the N-domain, suggesting that these structural elements must remain unfettered during FeEnt transit through FepA. The

44–111 pair, which was projected to link short helices in the N-domain (but showed no evidence of disulfide formation), did not inhibit FeEnt acquisition. In summary, each of the engineered Cys pairs in the N-domain that demonstrably formed a disulfide bond blocked FeEnt uptake through FepA.

Among Cys pairs that bridged the N- and C-domains of FepA, we previously engineered and characterized 14–300 (37). Residue I14C is situated in the TonB-box region of the N-domain; G300C is located on the periplasmic rim of the β -barrel in β -strand 7. Disulfide formation by 14–300 therefore precludes movement of the N-domain from the β -barrel, and accordingly, the 14–300 pair severely reduced FeEnt uptake in nutrition tests (Fig. 2, Fig. S2, and Table 1 (37)). Other inter-N–C Cys pairs produced less definitive effects. Six of them (42–162, 51–608, 128–463, 137–465, 138–445, and 149–180) showed normal halos of growth, even in the absence of β ME. Among these, 51–608, 128–463, 137–465, and 138–445 formed disulfide bonds that altered FepA's mobility in the gels/blots (Fig. 2A). These data indicated that tethering the N-domain to the β -barrel at these points did not prohibit FeEnt uptake. 42–162 and 149–180 showed no aberrant bands nor any inhibition of FeEnt uptake. The remaining inter-N–C Cys

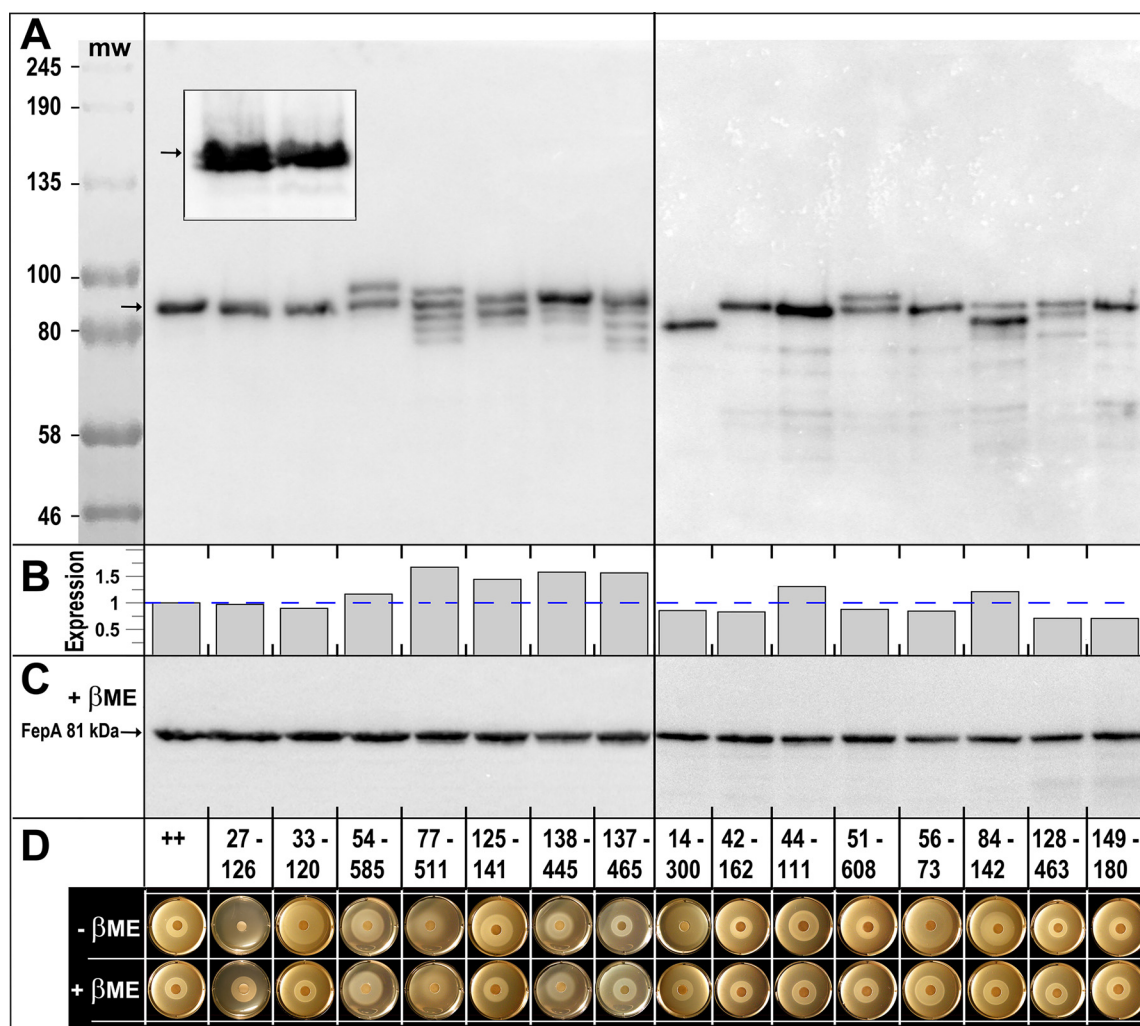


Figure 2. A, SDS-PAGE/western immunoblot analysis of disulfide formation by engineered Cys pairs. After growth of *E. coli* OKN3 harboring *fepA* mutants on the low-copy plasmid pHSG575 (75), in iron-deficient MOPS minimal media, we prepared cell-envelope fragments from *E. coli* OKN3 expressing WT FepA and each of the 15 Cys-pair mutants. We subjected the samples to SDS-PAGE (in the absence of any reducing agent), transferred the proteins to nitrocellulose, and performed western immunoblots with anti-FepA MAbs 41 and 45 (43), developed with ^{125}I -protein A (33). Five of the mutant proteins (33–120, 42–162, 44–111, 56–73, and 149–180) had the same electrophoretic mobility as native FepA: a single band at 81.5 kDa (76). Conversely, 10 of the mutant proteins showed single (14–300) or multiple (27–126, 54–585, 77–511, 125–141, 51–608, 84–142, 128–463, 137–465, and 138–445) immunoreactive bands with altered mobility, suggesting that they were fully or partially disulfide-bonded. The illustration derives from two separate immunoblots, separated by a vertical line. The gels also contained pre-stained molecular weight markers (New England Biolabs, catalog no. P77195) that we photographed on the nitrocellulose and added to the immunoblot images. The inset shows a magnified view, from another blot, of mutants 27–126 and 33–120. The former Cys pair forms two immunoreactive bands of nearly indistinguishable electrophoretic mobility, indicating that this Cys pair does form a disulfide bond. 33–120, conversely, migrates as a single band. B, quantification of FepA expression. The arrows in A, C, and the inset define the position of WT FepA that migrates at ~81 kDa (76). The immunoblot in A was developed with ^{125}I -protein A and scanned on a Typhoon Biomolecular imager, which allowed quantification of the immunoreactive material in each lane, using ImageJ (73). We normalized the expression values to the level of WT FepA (dashed blue line): Cys-pair mutant expression ranged from 0.71 to 1.67 of WT FepA expression; the mean expression among 15 mutants was 0.95 of WT FepA. C, we subjected the same samples as in A to reduction by 3 mM β ME, resolved them on a duplicate SDS-polyacrylamide gel, transferred the proteins to NC, and immunoblotted as described in A. This immunoblot, as well as that of A, contains WT FepA, that provides an internal molecular mass marker at 81.5 kDa. D, FeEnt nutrition tests in the absence and presence of β ME. We evaluated the ability of the WT FepA (+ +) and its Cys-pair mutants to acquire FeEnt in nonreducing or reducing conditions.

pairs, 54–585 and 77–511, produced slightly aberrant halos in the absence of β ME that did not revert to normal in the presence of β ME. The inability of the reducing agent to relieve inhibition complicated the interpretation of these Cys-pair mutants in the nutrition tests.

Effect of β ME on binding of ^{59}Fe Ent by FepA

Native *E. coli* FepA contains a single disulfide bond in L7 (Cys-487–Cys-494), which is needed for efficient transport of FeEnt (41, 43, 44). Because our experiments involved the reduction of engineered disulfide bonds in FepA, we determined

the effect of varying concentrations of β ME on ^{59}Fe Ent binding by OKN3 ($\Delta fepA$)/pITS23 (*fepA*⁺). The results (Fig. 3A) showed little impact of the reductant at concentrations <1 mM, but a 20% reduction in ^{59}Fe Ent binding capacity at 5 mM β ME.

Effect of engineered disulfide bonds on ^{59}Fe Ent transport

As in nutrition tests, all the engineered intra-N Cys pairs except 44–111 decreased the ^{59}Fe Ent uptake rate (V_{max}) (Fig. 3C). They inhibited ^{59}Fe Ent uptake to a level that was 25–30% of WT FepA, and β ME reversed their effects, reiterating that

Site-directed Cys pairs in FepA

Table 1
Attributes of Cys-pair mutants of FepA

Cys pair ^a	Location ^b	Expr ^c , −βME	S-S ^d , −βME	Siderophore nutrition ^e		[⁵⁹ Fe]Ent uptake ^f		FD sensor uptake ^g	
				−βME	+βME	−βME	+βME	−βME	+βME
None (++)	NA ^h	1.0	−	15	15	1.0	1.03	+++	++++
Intra-N-domain Cys pairs									
G27C:R126C	Nβ1–Nβ5	0.97	+	21	18	0.23	1.08	−	++
A33C:E120C	Nα2–Nβ5	0.90	+	28*	15	0.31	1.24	−	+++
D44C:T111C	Nα3–NL2	1.31	−	20	16	1.05	1.26	+++	+++
N56C:D73C	Nβ2–Nβ3	0.85	+	33*	20	0.19	0.99	−	+++
I84C:V142C	Nβ4–Nβ6	1.2	+	24	17	0.13	0.95	−	++
L125C:V141C	Nβ5–Nβ6	1.44	+	23	16	0.12	0.88	−	++
Inter-N-domain–C-domain Cys pairs									
I14C:G300C	TonB-box–β7	0.86	+	17*	15	0.03	1.03	−	−
A42C:N162C	Nα3–β1	0.83	−	15	15	ND ⁱ	ND	+++	ND
T51C:N608C	Nβ2–β18	0.88	+	15	16	0.57	0.74	+++	ND
G54C:T585C	Nβ2–β17	1.17	+	22	23	0.37	0.31	−	−
M77C:E511C	Nβ3–β14	1.67	+	21*	18*	0.57	0.48	+++	ND
P128C:A463C	Nβ5–β13	0.71	+	13	14	ND	ND	+++	ND
A137C:A465C	Nβ6–β13	1.57	+	14	15	ND	ND	+++	ND
A138C:A445C	Nβ6–β12	1.58	+	19	20	0.94	0.70	+++	ND
G149C:T180C	Nβ6–β2	0.71	−	15	15	ND	ND	+++	ND

^a Cys-pair mutants were engineered in wildtype FepA and carried on the pHSG575 (66) derivative pITS23 (39). Mutants identified in bold type showed severely impaired FeEnt uptake, unless exposed to βME.

^b We designed Cys pairs using the Modeller algorithm of CHIMERA (UCSF) and PDB file 1FEP (8).

^c Using ImageJ (73), we quantified the immunoreactive bands of each Cys-pair mutant in Fig. 2A, relative to the amount of wildtype FepA. Mean expression among 15 mutants was 0.96 of wildtype; the range of expression values was 0.71–1.67 of wildtype expression.

^d Evidence of disulfide formation, from observation of altered mobility in anti-FepA immunoblots of SDS-polyacrylamide gels of OM fractions, or reversible (*i.e.* relieved by βME) inhibition of FeEnt uptake.

^e The tabulated values are the diameters of the growth halo (41, 42) around a paper disk containing 50 μM FeEnt, after incubation at 37 °C overnight. Results marked with an asterisk (*) denote samples with a faint halo.

^f V_{max} values of [⁵⁹Fe]Ent uptake from V_{max} screening experiments were calculated relative to the rate of wildtype FepA (96 pmol/10⁹ cells/min; Fig. 3, C and D).

^g FeEnt uptake was measured as the rate of fluorescence recovery in FD sensor experiments, relative to wildtype FepA.

^h NA means not applicable.

ⁱ ND means no data.

disulfides within the N-domain interfere with [⁵⁹Fe]Ent transport. [⁵⁹Fe]Ent binding capacity was also lower in several of the Cys-pair mutants (Fig. 3B); for the most part, the addition of βME did not reverse this decrease (the exception was 84–142). In some cases, a lower [⁵⁹Fe]Ent-binding capacity contrasted with a relatively normal [⁵⁹Fe]Ent uptake rate (56–73 and 125–141, plus βME). But LGP turnover numbers are low (5.5/min (47)), so the extent of FepA saturation may not limit the uptake rate.

The impact of inter-N–C Cys pairs on [⁵⁹Fe]Ent uptake was more complicated. 14–300 nearly abolished [⁵⁹Fe]Ent uptake (29), but none of the others we assayed comparably inhibited acquisition of [⁵⁹Fe]Ent (Table 1). 54–585 decreased the FeEnt uptake rate by 65%, but other inter-N–C Cys pairs that we tested showed much less effect, in the range of 10–45%.

Fluorescent measurements of FeEnt uptake by Cys-pair mutants

Electrophoretic analyses did not always reveal disulfide bonds between Cys pairs, and most of the disulfides that we observed in SDS-PAGE/immunoblots were only partially formed. Consequently, the partial reductions in FeEnt uptake that we saw in nutrition tests and radioisotopic assays were difficult to interpret. We employed a fluorescent decoy (FD) sensor (30) to monitor TonB-dependent FeEnt uptake through FepA, as a better measure of whether the FeEnt uptake portal was open or held shut by engineered disulfide bonds. In a ΔtonB host (OKN13 (37)), FepA-FM (29) binds but cannot transport FeEnt. As a result, it becomes an FD sensor (30): the extent of its quenching reflects [FeEnt] and therefore the uptake of FeEnt

(*i.e.* its depletion) by other cells in the same solution. Incubation of FD sensor cells with the Cys-pair mutant cells allowed observations of the latter's ability to transport FeEnt, which appears as a reversal of FeEnt-mediated quenching (*i.e.* fluorescence recovery; Fig. 4). These data provided a quantitative time course of FepA's transport functionality.

The FD sensor provided more definitive data on the ability of the intra-N mutants of FepA to acquire FeEnt. Whereas transport of FeEnt by WT FepA quickly reverted the FeEnt-mediated quenching of the sensor, five of the six intra-N-domain Cys-pair mutants of FepA (27–126, 33–120, 56–73, 84–142, and 125–141) did not promote fluorescence recovery until we reduced their disulfides by adding βME to the cuvette. The only exception was 44–111, which supported fluorescence recovery like WT FepA, albeit at a slower rate. Given the uncertain status of the 44–111 disulfide bond, the fluorescence data either confirmed that it did not form or that its presence did not corrupt the FeEnt transport process. Overall, the results of the intra-N Cys pairs were consistent: disulfide formation in the N-domain prevented FeEnt transport, and reduction of those bonds restored the FeEnt uptake process.

Regarding inter-N–C Cys pairs, the FD sensor reiterated that the majority did not impair FeEnt uptake, despite that we observed disulfide bond formation by five of them. Cys-pair 77–511, which produced an inconclusive nutrition test with FeEnt, showed definitive transport in the FD sensor assay (Fig. 4 and Table 1). Overall, among the nine inter-N–C Cys pairs that we tested, besides 14–300, which falls into its own category, only 54–585 inhibited FeEnt transport in FD sensor assays. As

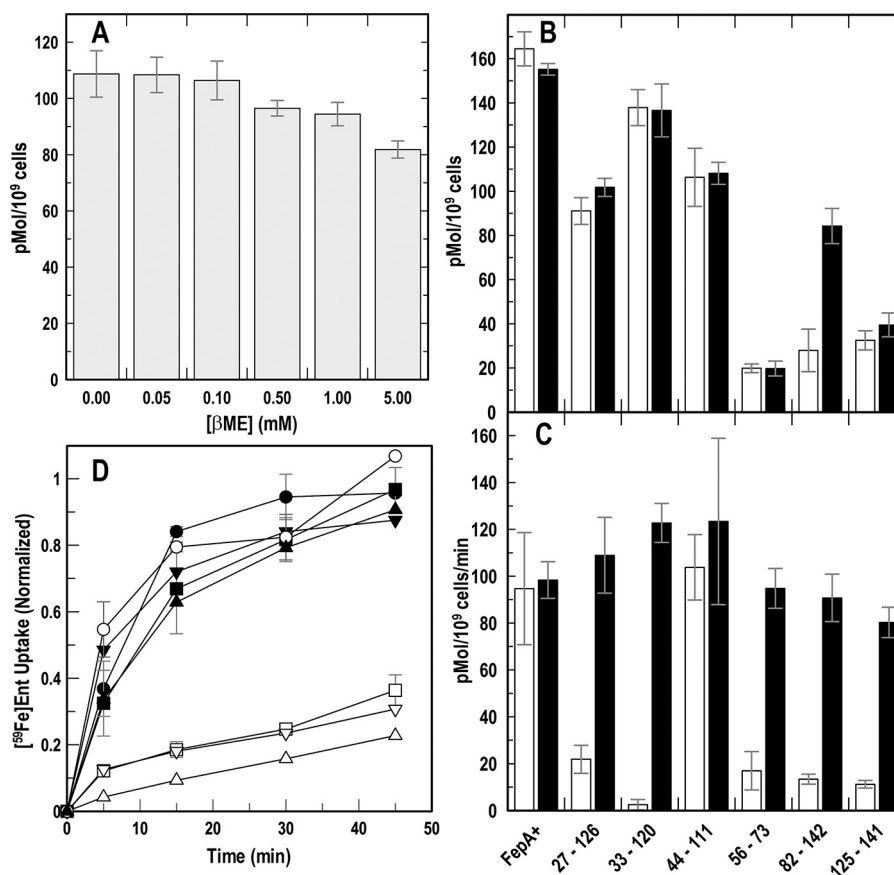


Figure 3. $[^{59}\text{Fe}]$ Ent binding and transport by intra-N Cys-pair mutants of FepA. After growth in iron-deficient MOPS medium, we tested *E. coli* expressing WT FepA or its Cys-pair mutants for binding and transport of $[^{59}\text{Fe}]$ Ent (74). *A*, effect of β ME on $[^{59}\text{Fe}]$ Ent binding to WT FepA. The FeEnt binding capacity of OKN3 ($\Delta fepA$)/pITS23 ($fepA^+$) slightly decreased (up to 20%) in the presence of 5 mM β ME. *B*, $[^{59}\text{Fe}]$ Ent binding to Cys-pair mutants: binding capacities in the presence of saturating (10 nM) $[^{59}\text{Fe}]$ Ent, in the absence or presence of 5 mM β ME. *C*, $[^{59}\text{Fe}]$ Ent uptake by Cys-pair mutants: V_{max} in the presence of saturating (10 nM) $[^{59}\text{Fe}]$ Ent, in the absence or presence of 5 mM β ME. *D*, accumulation of $[^{59}\text{Fe}]$ Ent: rates of $[^{59}\text{Fe}]$ Ent uptake in the absence (open symbols) and presence (filled symbols) of 5 mM β ME by WT FepA (\circ), 27–126 (\square), 33–120 (\triangle), and 125–141 (∇). β ME restored WT FeEnt uptake to all the intra-N Cys-pair mutants.

in nutrition tests, β ME did not relieve the inhibition of 54–585, confounding its interpretation.

In summary, we observed evidence of disulfide bond formation in 12 of the 15 Cys-pair mutants (Table 1). 10 FepA variants showed a band of altered electrophoretic mobility (Fig. 2A). Among the intra-N Cys pairs, 33–120, 44–111, and 56–73 showed no electrophoretic evidence of disulfide bond formation, but 33–120 and 56–73 reversibly (*i.e.* relieved by β ME) inhibited FeEnt utilization, indicating that they did bond. The observation of disulfide bond formation by intra-N Cys pairs always correlated with impaired FeEnt uptake (Table 1). Among inter-N–C Cys pairs, we saw anti-FepA-reactive bands with altered migration in all mutants except 42–162 and 149–180 (Fig. 2A and Table 1). In five of seven of these instances disulfide bond formation did not inhibit FeEnt uptake (Table 1). The exceptions (14–300 and 54–585) each had individual considerations that rationalized their behavior (discussed below).

Discussion

Delineation of the FepA transport mechanism requires insight into the actions of its N-domain during FeEnt internalization. In three disparate assays, the phenotypes of the Cys-pair mutants under investigation led to the same conclusion: intra-N disulfide bonds generally prevented FeEnt transport,

whereas inter-N–C disulfide bonds generally did not prevent FeEnt transport (Fig. 1). These data imply several conclusions. (i) The internal β -structure of the N-domain must rearrange during FeEnt uptake, because bonds that block such a transition also block transport. Disulfide bonds in the N-domain will restrict its potential motion, constraining conformational changes that are apparently required to achieve FeEnt import. (ii) The N-domain does not move out of the transmembrane pore as a folded rigid body (37), because bonds that hold it within the channel do not block FeEnt uptake. (iii) Numerous disulfide bonds that restrained the N-domain within the β -barrel did not prevent ligand uptake. These data suggest that most of the N terminus remains within the channel, which infers the formation of a transient pore (37) through which FeEnt passes into the periplasm.

It was a challenge to determine the extent of engineered disulfide bond formation *in vivo*. The Cys pairs produced a gamut of possible outcomes. Some formed disulfides that altered the R_f of FepA, whereas others did not change R_f , either because they did not form or because the disulfide did not alter migration in the gels. Even a single amino acid substitution may dramatically change the electrophoretic mobility of a protein (45), but the effects of engineered disulfides on the electrophoretic behavior of FepA were unpredictable: some created a

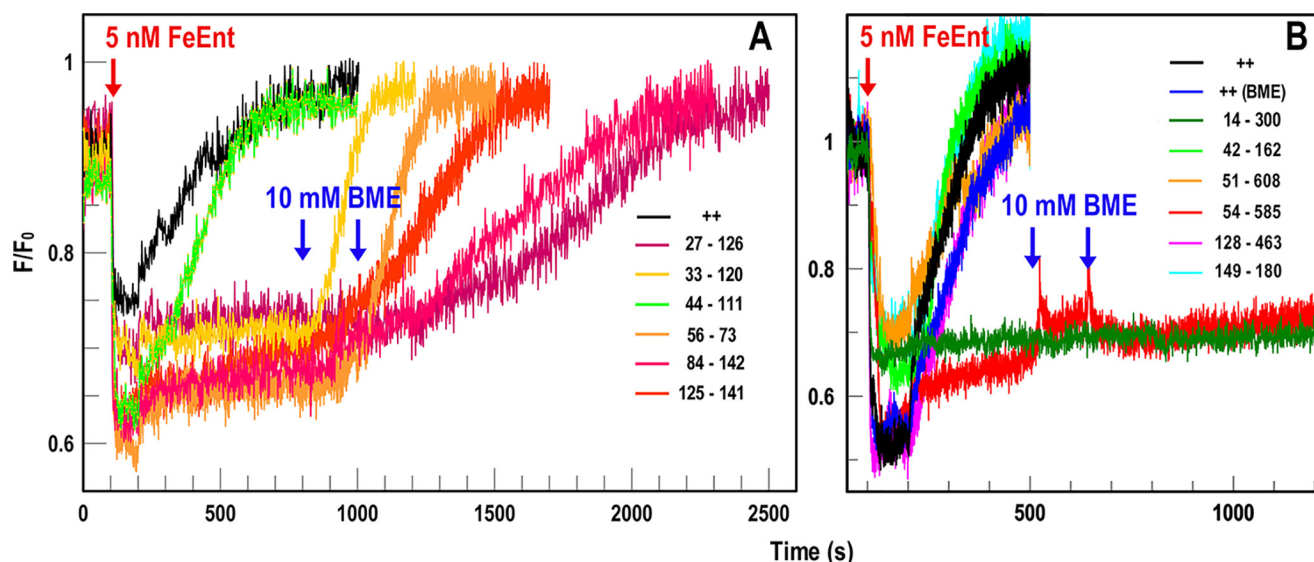


Figure 4. FD sensor measurements of FeEnt uptake by Cys-pair mutants of FepA. OKN3 expressing FepA with individual Cys pairs was incubated with the FD sensor OKN13 ($\Delta tonB$ and $\Delta fepA$)/pFepA-FM and observed in response to the addition of FeEnt (5 nM) at 37 °C. **A**, intra-N mutants. After quenching by addition of FeEnt at 100 s, WT FepA (++) and 44–111 conferred complete recovery (*i.e.* FeEnt uptake) within 500 s. Addition of 10 mM β ME at 800 s enabled recovery by 33–120, but all the remaining Cys pairs required a second aliquot of 10 mM β ME to confer recovery. **B**, inter-N and -C mutants. None of the Cys pairs prevented fluorescence recovery except 14–300 and 54–585, which were not affected by up to 20 mM β ME.

compact isoform of the denatured protein that moved faster, whereas others stabilized a larger isoform that moved slower. Anti-FepA immunoblots of 33–120 and 56–73 did not reveal any additional bands, despite the fact that both Cys pairs impaired FeEnt uptake and reverted to normal transport when reduced by β ME. Hence, disulfides formed in both 33–120 and 56–73, but the immunoblots did not reveal them. Furthermore, when we observed a Cys pair mutant band with different R_f values, usually only $\sim 50\%$ of the protein was in the altered state. The engineered Cys-pair sulfhydryls were hypothetically close enough (<2.5 Å between sulfur atoms (8)) to form disulfides, but without the crystallographic data on each mutant protein their impact on local folding and side-chain projection was unknown. Furthermore, for numerous engineered Cys pairs the DsbAB system (46–50) did not efficiently oxidize disulfide bond formation, as evidenced by the susceptibility of the component sulfhydryls to alkylation by FM. Finally, we saw multiple immunoreactive electrophoretic forms of some FepA Cys-pair mutants. Besides fully synthesized, secreted, and folded OM proteins, immunoblots may reveal nascent or incomplete mutant proteins, in a pre- or post-disulfide-bonded state, which may explain some of the multiple bands. Overall, the electrophoretic studies of Cys-pair mutants were informative, but insufficient to quantify the extent of disulfide formation or to explain the nature of each immunoreactive band.

The intrinsic disulfide in FepA L7 (C487–C494) was another complication, which raised the possibility of aberrant disulfides with engineered Cys sulfhydryls. However, C487–C494 is a stable bond; without reduction, residues C487 and C494 are unreactive with methane thiosulfonate or maleimide probes (Fig. S2A) (29, 39, 41, 51). Furthermore, the L7 disulfide is essential to transport activity: substitutions C487S, C494S, and their combined double-mutant all abrogate FeEnt uptake (data not shown). Consequently, if engineered Cys residues erroneously bond with either native Cys, blocking formation of C487–C494,

then FeEnt uptake will diminish. We did not observe that result with the single mutants we generated herein (Fig. S2), nor with >25 other individual Cys substitutions in FepA, at diverse locations in its primary structure (29, 30, 37, 51). So, it is unlikely that the Cys-pair sulfhydryls we engineered formed incorrect disulfides with C487 and C494. The native cysteines are separated by only six residues in L7 and probably immediately bond as that region of the polypeptide exits the ribosome and folds.

FD sensor assays provided unique, real-time insight into the transport behavior of the FepA mutants. Nutrition tests and [59 Fe]Ent uptake assays were useful but sometimes hard to interpret, whereas FD assays were unambiguous about the impact of each Cys pair on FeEnt transport. The sensor cell OKN13/pFepA-FM depicted uptake of FeEnt by the FepA Cys-pair mutants *in vivo*. It showed that except for 44–111 (which did not form a disulfide bond), all intra-N Cys pairs blocked FeEnt uptake until exposed to 10 mM β ME. Conversely, with the exception of 14–300 and 54–585, none of the other seven inter-N–C Cys pairs inhibited FeEnt uptake. Cys pair 14–300 is unique among all the mutants, because its immobilization of the TonB-box both holds the N-domain within the β -barrel and interferes with signal transduction to TonB. 54–585 blocked FeEnt uptake, but its inhibition was not reversed by β ME, suggesting that its negative phenotype was unrelated to disulfide formation. Despite these two exceptions, the more definitive FD sensors corroborated and clarified the siderophore nutrition and [59 Fe]Ent accumulation results.

The crystal structures of ligand-free and ligand-bound transporters (9–12, 28, 32) revealed that when LGP adsorbs metal complexes by induced fit (29), subtle changes propagate through their N termini that alter the disposition of residues in the periplasm, promoting interactions with the TonB C terminus (34, 35). These dynamics raise the possibility that intra-N disulfides interfere with FeEnt uptake because they corrupt signal transduction to TonBExbBD. However, inspection of the

ligand-free and ligand-bound forms of FhuA, FecA, and BtuB show little or no deviation in the regions of the N-domain that contain the Cys pairs we engineered in FepA. We cannot exclude the notion that intra-N Cys pairs interfere with signal transduction to TonBExbBD, but this explanation seems unlikely.

Despite the importance of TonB-dependent iron acquisition to Gram (–) bacterial pathogenesis (52–61) and the solution of many LGP crystal structures (FepA (8), Cir (8), FhuA (11, 12), FecA (11, 12), FoxA (32), BtuB (9), FptA (62), FpvA (63), PfeA (28), and FyuA (64)), it is unknown how metal complexes move through their channels or how the actions of TonB facilitate uptake. Biochemical data on FepA (65) and crystallographic studies of other LGPs (28, 32) indicated a two-site model during FeEnt adsorption. Other approaches, including site-directed alkylation of FepA during FeEnt transport (37) and molecular dynamics simulations of the interaction between TonB and BtuB (36), suggested that the N-domain globules of LGP exit their transmembrane β -barrels, either stably folded or by unfolding into the periplasm. Our results argue against both these mechanisms. First, seven of nine inter-N–C Cys pairs that we tested did not inhibit FeEnt uptake, refuting the notion that the N-domain exits the β -barrel as an intact globule. Second, tethering Cys residues at 51, 77, 128, 137, or 138 to the β -barrel (verified by immunoblot) did not prevent transport, which supports the alternative idea that the N-domain remains within the pore as FeEnt enters. It is now apparent that conformational motion *within* the N-domain is indispensable to the uptake reaction, because five of six the intra-N domain Cys pairs we created prevented FeEnt internalization, unless exposed to β ME.

Experimental procedures

Bacterial strains, plasmids, and culture conditions

Plasmid pITS23 (39, 40) is a derivative of pHSG575 (66) that carries *fepA*⁺ under the control of its natural Fur-regulated promoter. We engineered Cys-pair alleles of *fepA* in this vector. Derivatives of BN1071 (67) with precise deletions (OKN1, Δ tonB; OKN3, Δ fepA; and OKN13, Δ tonB, Δ fepA (37)), harboring variants of pITS23 that encode WT or mutant alleles, were grown at 37 °C with shaking to stationary phase in Luria-Bertani (LB) broth. We added streptomycin (100 μ g/ml) to the growth media and chloramphenicol (20 μ g/ml) to select for the plasmids when appropriate. We de-repressed the FeEnt transport system by subculturing bacteria from stationary phase LB cultures at 1% into iron-deficient MOPS minimal medium (68) and shaking at 200 rpm for 5.5–6 h at 37 °C, until cell density reached an absorbance at 600 nm of 0.8–0.9.

Site-directed mutagenesis of *E. coli fepA*

We used QuikChange (Stratagene) for single- and double-Cys substitutions in FepA, using complementary oligonucleotides flanking the mutation, followed by digestion of the WT vector by DpnI. We confirmed the mutations by sequencing (Genesys, Daly City, CA) of purified plasmids.

Intra-N Cys pairs—We constructed six Cys pairs (G27C-R126C, A33C-E120C, D44C-T111C, N56C-D73C, I84C-V142C, and L125C-V141C) in different regions of the N-do-

main of FepA. Each pair may form a disulfide bond within the globular domain, which prevents separation of its constituent β -strands (Fig. 1 and Table 1).

Inter-N–C Cys pairs—We analyzed another group of nine Cys pairs (I14C-G300C, A42C-N162C, T51C-N608C, G54C-T585C, M77C-E511C, P128C-A463C, A137C-A465C, A138C-A445C, and G149C-T180C) in which one sulfhydryl was on the surface of the N-domain and a second was on the internal wall of the FepA β -barrel (Fig. 1 and Table 1).

Siderophores

We purified enterobactin from *E. coli* and formed the iron(III) complex with ⁵⁶Fe or ⁵⁹Fe (33) and chromatographically-purified FeEnt over Sephadex LH20 (42). We stored the [⁵⁶Fe]Ent and [⁵⁹Fe]Ent complexes on ice and re-purified them over LH20 to remove oxidized and degraded compounds when $A_{393\text{ nm}}/A_{495\text{ nm}}$ exceeded 0.7.

Siderophore nutrition tests

To qualitatively evaluate the FeEnt uptake abilities encoded by the mutant *fepA* alleles, we performed siderophore nutrition tests (42, 44). We expressed the results as the diameter of bacterial growth around the paper disk, and we compared mutant halos to the growth halo conferred by a strain harboring pITS23 (*fepA*⁺). To test the effect of disulfide bond reduction on FeEnt transport by the FepA mutants, we added 1 mM β ME to the molten agar.

Preparation of cell-envelope fractions

After growth in LB broth overnight, we sub-cultured FepA Cys-pair mutant derivatives of OKN3/pITS23 at (1%) into 20 ml of iron-deficient MOPS media, and we incubated the cultures with shaking for 5.5–6 h at 37 °C, to an $A_{600\text{ nm}} = 1\text{--}1.2$ ($5\text{--}6 \times 10^8$ cells/ml). We collected the cells by centrifugation at $7500 \times g$, resuspended the pellets in 2 ml of PBS containing trace amounts of DNase and RNase, and passed the cell suspensions (three times) through a French pressure cell at 14,000 p.s.i. (69). After spinning the lysates at $3000 \times g$ for 10 min to remove unbroken cells and debris, we transferred the supernatants to microcentrifuge tubes and pelleted the cell envelopes by centrifugation at $13,000 \times g$ for 45 min. We resuspended the cell envelopes in 400 μ l of 50 mM NaHPO₄, pH 6.7, containing 1% SDS, added 3% β ME to one-half of the sample (reduced), left the remainder unaltered (nonreduced), and denatured the proteins in both samples by boiling for 5 min.

Electrophoresis and western immunoblots

We electrophoretically and immunochemically analyzed cell-envelope fractions of the mutants. For SDS-PAGE (70, 71), we suspended 30 μ g of cell-envelope protein (measured by UV absorbance) in sample buffer (containing 1% SDS), with or without 3% β ME, boiled the sample for 5 min, and resolved the samples by SDS-PAGE at 30 mA. To enhance the separation of proteins in the 80-kDa range, we continued electrophoresis at 30 mA for an additional 45 min after the tracking dye left the gels. To visualize FepA in western immunoblots, we electrophoretically transferred the proteins from the SDS-polyacrylamide gels to nitrocellulose (NC) paper, blocked the paper with

Site-directed Cys pairs in FepA

1% gelatin in 50 mM Tris chloride, pH 7.4, 0.9% NaCl (TBSG), and incubated with a mixture of anti-FepA mouse monoclonal antibodies (mAbs) 41 and 45 (72), both of which have Ig2b heavy chains, in the same buffer. After incubation with the antisera for 1 h at room temperature, we washed the NC five times with 0.5% Tween 20 in TBS, incubated it with ^{125}I -protein A in TBSG for 1 h at room temperature, washed with three rinses of tap water, dried the paper, and visualized the adsorbed ^{125}I -protein A on a Typhoon 8600 Biomolecular Scanner (GE/Amersham Biosciences).

Labeling reactions with FM

We estimated the extent of disulfide formation in Cys-pair mutants of FepA by modifying them with FM. We precipitated 100 μl of the denatured, reduced, and nonreduced cell-envelope samples described above with 7 volumes of ice-cold acetone, and after incubation at -20°C for 2 h, we pelleted the proteins by centrifugation at $13,000 \times g$ for 5 min and washed the pellets twice with ice-cold 70% acetone. We resuspended the reduced and nonreduced cell-envelope proteins in 50 mM NaH_2PO_4 , pH 6.7, containing 1% SDS, added FM to 5 μM , incubated for 15 min at 37°C (29), and stopped the labeling reactions by precipitation with ice-cold acetone as described above. We washed the samples with ice-cold 70% acetone, solubilized them with SDS-PAGE sample buffer, and subjected them to SDS-PAGE/Western immunoblot.

Image analysis

We analyzed images from SDS-polyacrylamide gels of fluoresceinated proteins and from phosphorimager of ^{125}I -protein A immunoblots, collected on a Typhoon Biomolecular scanner (GE Healthcare) using ImageJ (73).

Effect of βME on FeEnt binding by FepA

Because in several experiments we used βME to reduce disulfide bonds within FepA, we tested its effects on the adsorption of ^{59}Fe Ent by OKN3/pITS23 (*fepA*⁺). We grew the bacteria in LB overnight, subcultured at 1% in iron-deficient MOPS minimal medium, shook the cultures for 5 h at 37°C , added βME at increasing concentrations to 5 mM, and shook the cultures for additional 30 min at 37°C . We created a duplicate control culture that we subjected to the same conditions, but without any βME . To determine the ^{59}Fe Ent-binding capacities, we added the ferric siderophore at 10 nM, filtered the cells after 1 min, washed the filters with 10 ml of 0.9% LiCl, and determined the amount of adsorbed radioactivity in a Packard gamma counter. The parent host strain (OKN3, ΔfepA) does not adsorb ^{59}Fe Ent. We employed it in these binding studies as a negative (background) control.

Ferric enterobactin accumulation

We subcultured overnight LB cultures at 1% in iron-deficient MOPS medium with appropriate antibiotics and continued growth at 37°C with shaking for 5.5 h. In some cases, the bacteria were exposed to 5 mM βME in the final 30 min of growth. We next added ^{59}Fe Ent to 3-ml aliquots of the cells at 37°C (in the original culture medium) to a final concentration of 10 μM , removed 100- μl aliquots at 5, 10, 15, 30, and 45 min, filtered

them, and washed them with 10 ml of 0.9% LiCl, and we determined the amounts of ^{59}Fe on the filters in a Packard gamma counter. For each accumulation experiment, we collected triplicate samples at each time point and averaged the data. At a density of $\sim 5 \times 10^8$ cells/ml, the added ^{59}Fe Ent was sufficient to remain in excess for more than 2 h of transport at V_{max} (74).

Fluorescence assays of FeEnt transport

We employed FD sensors (30) to monitor TonB-dependent FeEnt uptake through FepA, as a measure of whether the FeEnt uptake portal was open or held shut by engineered disulfide bonds. In this approach, we used the transport-defective host strain OKN13 (ΔtonB and ΔfepA) harboring a plasmid (pITS23) encoding *fepA* with a single amino acid substitution (A698C), which was modifiable by FM (FepA_A698C-FM; henceforth called FepA-FM). OKN13/pFepA-FM bound FeEnt, which quenched its fluorescence (29), but its TonB deficiency prevented it from transporting the bound iron complex. The absence of TonB transformed the fluoresceinated bacteria into spectroscopic sensors of [FeEnt] (30); if transport-competent cells cohabited the same environment, then the emissions of OKN13/pFepA-FM reflected their FeEnt uptake activity. Hence, in fluorescence spectroscopic uptake studies, OKN13/pFepA-FM was a decoy sensor that monitored FeEnt uptake by the FepA Cys-pair mutants in a host strain OKN3 (ΔfepA). These data provided a quantitative time course of FepA's transport functionality.

For each assay, we used 50 μl of OKN13/pFepA-FM (44) at 5×10^8 cells/ml. We analyzed the aliquot in 2 ml of PBS + 0.4% glucose at 37°C , and we recorded its fluorescence intensity for 100 s, before adding FeEnt to the cuvette at a final concentration of 5 nM. We incubated the sample for 100 s, during which time fluorescence was quenched ($\sim 60\%$ quenching for FepA labeled at position A698C), and we then added 50 μl of the test strain ($\sim 5 \times 10^6$ cells) at 200 s while monitoring fluorescence. If no increase in fluorescence occurred (indicating lack of uptake) by 800 s, we added βME to a final concentration of 10 mM. For some strains, we added a second aliquot of βME at 1000 s that raised the final concentration to 20 mM.

Author contributions—A. M., V. T., K. J. M., C. R. S., D. C. S., S. M. N., and P. E. K. conceptualization; A. M. and P. E. K. resources; A. M., V. T., S. M. N., and P. E. K. data curation; A. M., V. T., S. M. N., and P. E. K. formal analysis; A. M., S. M. N., and P. E. K. supervision; A. M. and P. E. K. funding acquisition; A. M. and P. E. K. validation; A. M., V. T., K. J. M., C. R. S., A. K., T. Y., D. C. S., N. J. L., S. M. N., and P. E. K. investigation; A. M., V. T., K. J. M., C. R. S., D. C. S., N. J. L., S. M. N., and P. E. K. methodology; A. M. and P. E. K. writing-original draft; A. M., S. M. N., and P. E. K. project administration; A. M. and P. E. K. writing-review and editing.

Acknowledgment—We thank Ron Kaback for helpful discussions about the experiments.

References

1. Cowan, S. W., Schirmer, T., Rummel, G., Steiert, M., Ghosh, R., Paupit, R. A., Jansonius, J. N., and Rosenbusch, J. P. (1992) Crystal structures explain functional properties of two *E. coli* porins. *Nature* **358**, 727–733 [CrossRef Medline](#)

2. Weiss, M. S., Wacker, T., Weckesser, J., Welte, W., and Schulz, G. E. (1990) The three-dimensional structure of porin from *Rhodobacter capsulatus* at 3 Å resolution. *FEBS Lett.* **267**, 268–272 [CrossRef Medline](#)
3. Nikaido, H., and Rosenberg, E. Y. (1981) Effect on solute size on diffusion rates through the transmembrane pores of the outer membrane of *Escherichia coli*. *J. Gen. Physiol.* **77**, 121–135 [CrossRef Medline](#)
4. Nikaido, H., and Vaara, M. (1985) Molecular basis of bacterial outer membrane permeability. *Microbiol. Rev.* **49**, 1–32 [CrossRef Medline](#)
5. Schirmer, T., Keller, T. A., Wang, Y. F., and Rosenbusch, J. P. (1995) Structural basis for sugar translocation through maltoporin channels at 3.1 Å resolution (see comments). *Science* **267**, 512–514 [CrossRef Medline](#)
6. Klebba, P. E., Hofnung, M., and Charbit, A. (1994) A model of maltodextrin transport through the sugar-specific porin, LamB, based on deletion analysis. *EMBO J.* **13**, 4670–4675 [CrossRef Medline](#)
7. Luckey, M., and Nikaido, H. (1980) Diffusion of solutes through channels produced by phage λ receptor protein of *Escherichia coli*: inhibition by higher oligosaccharides of maltose series. *Biochem. Biophys. Res. Commun.* **93**, 166–171 [CrossRef Medline](#)
8. Buchanan, S. K., Smith, B. S., Venkatramani, L., Xia, D., Esser, L., Palnitkar, M., Chakraborty, R., van der Helm, D., and Deisenhofer, J. (1999) Crystal structure of the outer membrane active transporter FepA from *Escherichia coli* (see comments). *Nat. Struct. Biol.* **6**, 56–63 [CrossRef Medline](#)
9. Chimento, D. P., Mohanty, A. K., Kadner, R. J., and Wiener, M. C. (2003) Substrate-induced transmembrane signaling in the cobalamin transporter BtuB. *Nat. Struct. Biol.* **10**, 394–401 [CrossRef Medline](#)
10. Ferguson, A. D., Chakraborty, R., Smith, B. S., Esser, L., van der Helm, D., and Deisenhofer, J. (2002) Structural basis of gating by the outer membrane transporter FecA. *Science* **295**, 1715–1719 [CrossRef Medline](#)
11. Ferguson, A. D., Hofmann, E., Coulton, J. W., Diederichs, K., and Welte, W. (1998) Siderophore-mediated iron transport: crystal structure of FhuA with bound lipopolysaccharide (see comments). *Science* **282**, 2215–2220 [CrossRef Medline](#)
12. Locher, K. P., Rees, B., Koebnik, R., Mitschler, A., Moulinier, L., Rosenbusch, J. P., and Moras, D. (1998) Transmembrane signaling across the ligand-gated FhuA receptor: crystal structures of free and ferrichrome-bound states reveal allosteric changes. *Cell* **95**, 771–778 [CrossRef Medline](#)
13. Jordan, L. D., Zhou, Y., Smallwood, C. R., Lill, Y., Ritchie, K., Yip, W. T., Newton, S. M., and Klebba, P. E. (2013) Energy-dependent motion of TonB in the Gram-negative bacterial inner membrane. *Proc. Natl. Acad. Sci. U.S.A.* **110**, 11553–11558 [CrossRef Medline](#)
14. Schauer, K., Rodionov, D. A., and de Reuse, H. (2008) New substrates for TonB-dependent transport: do we only see the 'tip of the iceberg'? *Trends Biochem. Sci.* **33**, 330–338 [CrossRef Medline](#)
15. le Coutre, J., and Kaback, H. K. (2000) Structure-function relationships of integral membrane proteins: membrane transporters vs. channels. *Biopolymers* **55**, 297–307 [CrossRef Medline](#)
16. Saier, M. H., Jr. (2000) Families of proteins forming transmembrane channels. *J. Membr. Biol.* **175**, 165–180 [CrossRef Medline](#)
17. Zhai, Y. F., Heijne, W., and Saier, M. H., Jr. (2003) Molecular modeling of the bacterial outer membrane receptor energizer, ExbBD/TonB, based on homology with the flagellar motor, MotAB. *Biochim. Biophys. Acta* **1614**, 201–210 [CrossRef Medline](#)
18. Rutz, J. M., Liu, J., Lyons, J. A., Goranson, J., Armstrong, S. K., McIntosh, M. A., Feix, J. B., and Klebba, P. E. (1992) Formation of a gated channel by a ligand-specific transport protein in the bacterial outer membrane. *Science* **258**, 471–475 [CrossRef Medline](#)
19. Nikaido, H., and Rosenberg, E. Y. (1983) Porin channels in *Escherichia coli*: studies with liposomes reconstituted from purified proteins. *J. Bacteriol.* **153**, 241–252 [CrossRef Medline](#)
20. Luckey, M., and Nikaido, H. (1980) Specificity of diffusion channels produced by λ phage receptor protein of *Escherichia coli*. *Proc. Natl. Acad. Sci. U.S.A.* **77**, 167–171 [CrossRef Medline](#)
21. Noinaj, N., Guillier, M., Barnard, T. J., and Buchanan, S. K. (2010) TonB-dependent transporters: regulation, structure, and function. *Annu. Rev. Microbiol.* **64**, 43–60 [CrossRef Medline](#)
22. Eisenbeis, S., Lohmiller, S., Valdebenito, M., Leicht, S., and Braun, V. (2008) NagA-dependent uptake of *N*-acetyl-glucosamine and *N*-acetyl-chitin oligosaccharides across the outer membrane of *Caulobacter crescentus*. *J. Bacteriol.* **190**, 5230–5238 [CrossRef Medline](#)
23. Lohmiller, S., Hantke, K., Patzer, S. I., and Braun, V. (2008) TonB-dependent maltose transport by *Caulobacter crescentus*. *Microbiology* **154**, 1748–1754 [CrossRef Medline](#)
24. Neugebauer, H., Herrmann, C., Kammer, W., Schwarz, G., Nordheim, A., and Braun, V. (2005) ExbBD-dependent transport of maltodextrins through the novel MalA protein across the outer membrane of *Caulobacter crescentus*. *J. Bacteriol.* **187**, 8300–8311 [CrossRef Medline](#)
25. Fetherston, J. D., Kirillina, O., Bobrov, A. G., Paulley, J. T., and Perry, R. D. (2010) The yersiniabactin transport system is critical for the pathogenesis of bubonic and pneumonic plague. *Infect. Immun.* **78**, 2045–2052 [CrossRef Medline](#)
26. Larson, J. A., Higashi, D. L., Stojilkovic, I., and So, M. (2002) Replication of *Neisseria meningitidis* within epithelial cells requires TonB-dependent acquisition of host cell iron. *Infect. Immun.* **70**, 1461–1467 [CrossRef Medline](#)
27. Nairn, B. L., Eliasson, O. S., Hyder, D. R., Long, N. J., Majumdar, A., Chakravorty, S., McDonald, P., Roy, A., Newton, S. M., and Klebba, P. E. (2017) Fluorescence high-throughput screening for inhibitors of TonB action. *J. Bacteriol.* **199**, e00889-16 [CrossRef Medline](#)
28. Moynié, L., Milenkovic, S., Mislin, G. L. A., Gasser, V., Mallocci, G., Baco, E., McCaughan, R. P., Page, M. G. P., Schalk, I. J., Ceccarelli, M., and Naismith, J. H. (2019) The complex of ferric-enterobactin with its transporter from *Pseudomonas aeruginosa* suggests a two-site model. *Nat. Commun.* **10**, 3673 [CrossRef Medline](#)
29. Smallwood, C. R., Jordan, L., Trinh, V., Schuerch, D. W., Gala, A., Hanson, M., Hanson, M., Shipelskiy, Y., Majumdar, A., Newton, S. M., and Klebba, P. E. (2014) Concerted loop motion triggers induced fit of FepA to ferric enterobactin. *J. Gen. Physiol.* **144**, 71–80 [CrossRef Medline](#)
30. Chakravorty, S., Shipelskiy, Y., Kumar, A., Majumdar, A., Yang, T., Nairn, B. L., Newton, S. M., and Klebba, P. E. (2019) Universal fluorescent sensors of high affinity iron transport, applied to ESKAPE(yen) pathogens. *J. Biol. Chem.* **294**, 4682–4692 [CrossRef Medline](#)
31. Di Masi, D. R., White, J. C., Schnaitman, C. A., and Bradbeer, C. (1973) Transport of vitamin B12 in *Escherichia coli*: common receptor sites for vitamin B12 and the E colicins on the outer membrane of the cell envelope. *J. Bacteriol.* **115**, 506–513 [CrossRef Medline](#)
32. Josts, I., Veith, K., and Tidow, H. (2019) Ternary structure of the outer membrane transporter FoxA with resolved signalling domain provides insights into TonB-mediated siderophore uptake. *Elife* **8**, e48528 [CrossRef Medline](#)
33. Newton, S. M., Trinh, V., Pi, H., and Klebba, P. E. (2010) Direct measurements of the outer membrane stage of ferric enterobactin transport: postuptake binding. *J. Biol. Chem.* **285**, 17488–17497 [CrossRef Medline](#)
34. Pawelek, P. D., Croteau, N., Ng-Thow-Hing, C., Khursigara, C. M., Moiseeva, N., Allaire, M., and Coulton, J. W. (2006) Structure of TonB in complex with FhuA, *E. coli* outer membrane receptor. *Science* **312**, 1399–1402 [CrossRef Medline](#)
35. Shultis, D. D., Purdy, M. D., Banchs, C. N., and Wiener, M. C. (2006) Outer membrane active transport: structure of the BtuB:TonB complex. *Science* **312**, 1396–1399 [CrossRef Medline](#)
36. Gumbart, J., Wiener, M. C., and Tajkhorshid, E. (2007) Mechanics of force propagation in TonB-dependent outer membrane transport. *Biophys. J.* **93**, 496–504 [CrossRef Medline](#)
37. Ma, L., Kaserer, W., Annamalai, R., Scott, D. C., Jin, B., Jiang, X., Xiao, Q., Maymani, H., Massis, L. M., Ferreira, L. C., Newton, S. M., and Klebba, P. E. (2007) Evidence of ball-and-chain transport of ferric enterobactin through FepA. *J. Biol. Chem.* **282**, 397–406 [CrossRef Medline](#)
38. Cao, Z., and Klebba, P. E. (2002) Mechanisms of colicin binding and transport through outer membrane porins. *Biochimie* **84**, 399–412 [CrossRef Medline](#)
39. Smallwood, C. R., Marco, A. G., Xiao, Q., Trinh, V., Newton, S. M., and Klebba, P. E. (2009) Fluoresceination of FepA during colicin B killing: effects of temperature, toxin and TonB. *Mol. Microbiol.* **72**, 1171–1180 [CrossRef Medline](#)
40. Scott, D. C., Cao, Z., Qi, Z., Bauler, M., Igo, J. D., Newton, S. M., and Klebba, P. E. (2001) Exchangeability of N termini in the ligand-gated

Site-directed Cys pairs in FepA

- porins of *Escherichia coli*. *J. Biol. Chem.* **276**, 13025–13033 [CrossRef Medline](#)
41. Liu, J., Rutz, J. M., Klebba, P. E., and Feix, J. B. (1994) A site-directed spin-labeling study of ligand-induced conformational change in the ferric enterobactin receptor, FepA. *Biochemistry* **33**, 13274–13283 [CrossRef Medline](#)
 42. Wayne, R., Frick, K., and Neilands, J. B. (1976) Siderophore protection against colicins M, B, V, and Ia in *Escherichia coli*. *J. Bacteriol.* **126**, 7–12 [CrossRef Medline](#)
 43. Annamalai, R., Jin, B., Cao, Z., Newton, S. M., and Klebba, P. E. (2004) Recognition of ferric catecholates by FepA. *J. Bacteriol.* **186**, 3578–3589 [CrossRef Medline](#)
 44. Cao, Z., Qi, Z., Sprencel, C., Newton, S. M., and Klebba, P. E. (2000) Aromatic components of two ferric enterobactin binding sites in *Escherichia coli* fepA. *Mol. Microbiol.* **37**, 1306–1317 [CrossRef Medline](#)
 45. Noel, D., Nikaido, K., and Ames, G. F. (1979) A single amino acid substitution in a histidine-transport protein drastically alters its mobility in sodium dodecyl sulfate-polyacrylamide gel electrophoresis. *Biochemistry* **18**, 4159–4165 [CrossRef Medline](#)
 46. Bardwell, J. C. (1994) Building bridges: disulphide bond formation in the cell. *Mol. Microbiol.* **14**, 199–205 [CrossRef Medline](#)
 47. Gleiter, S., and Bardwell, J. C. (2008) Disulfide bond isomerization in prokaryotes. *Biochim. Biophys. Acta* **1783**, 530–534 [CrossRef Medline](#)
 48. Goldstone, D., Haebel, P. W., Katzen, F., Bader, M. W., Bardwell, J. C., Beckwith, J., and Metcalf, P. (2001) DsbC activation by the N-terminal domain of DsbD. *Proc. Natl. Acad. Sci. U.S.A.* **98**, 9551–9556 [CrossRef Medline](#)
 49. Mamathambika, B. S., and Bardwell, J. C. (2008) Disulfide-linked protein folding pathways. *Annu. Rev. Cell Dev. Biol.* **24**, 211–235 [CrossRef Medline](#)
 50. Tapley, T. L., Eichner, T., Gleiter, S., Ballou, D. P., and Bardwell, J. C. (2007) Kinetic characterization of the disulfide bond-forming enzyme DsbB. *J. Biol. Chem.* **282**, 10263–10271 [CrossRef Medline](#)
 51. Cao, Z., Warfel, P., Newton, S. M., and Klebba, P. E. (2003) Spectroscopic observations of ferric enterobactin transport. *J. Biol. Chem.* **278**, 1022–1028 [CrossRef Medline](#)
 52. Buckling, A., Harrison, F., Vos, M., Brockhurst, M. A., Gardner, A., West, S. A., and Griffin, A. (2007) Siderophore-mediated cooperation and virulence in *Pseudomonas aeruginosa*. *FEMS Microbiol. Ecol.* **62**, 135–141 [CrossRef Medline](#)
 53. Cornelissen, C. N., and Hollander, A. (2011) TonB-dependent transporters expressed by *Neisseria gonorrhoeae*. *Front. Microbiol.* **2**, 117 [CrossRef Medline](#)
 54. Dhople, A. M., Ibanez, M. A., and Poirier, T. C. (1996) Role of iron in the pathogenesis of *Mycobacterium avium* infection in mice. *Microbios* **87**, 77–87 [Medline](#)
 55. Furman, M., Fica, A., Saxena, M., Di Fabio, J. L., and Cabello, F. C. (1994) *Salmonella typhi* iron uptake mutants are attenuated in mice. *Infect. Immun.* **62**, 4091–4094 [CrossRef Medline](#)
 56. Konings, A. F., Martin, L. W., Sharples, K. J., Roddam, L. F., Latham, R., Reid, D. W., and Lamont, I. L. (2013) *Pseudomonas aeruginosa* uses multiple pathways to acquire iron during chronic infection in cystic fibrosis lungs. *Infect. Immun.* **81**, 2697–2704 [CrossRef Medline](#)
 57. Mortensen, B. L., and Skaar, E. P. (2013) The contribution of nutrient metal acquisition and metabolism to *Acinetobacter baumannii* survival within the host. *Front. Cell Infect. Microbiol.* **3**, 95 [CrossRef Medline](#)
 58. Schoolnik, G. K. (2002) Microarray analysis of bacterial pathogenicity. *Adv. Microb. Physiol.* **46**, 1–45 [CrossRef Medline](#)
 59. Smith, K. D. (2007) Iron metabolism at the host pathogen interface: lipocalin 2 and the pathogen-associated iroA gene cluster. *Int. J. Biochem. Cell Biol.* **39**, 1776–1780 [CrossRef Medline](#)
 60. Torres, A. G., Redford, P., Welch, R. A., and Payne, S. M. (2001) TonB-dependent systems of uropathogenic *Escherichia coli*: aerobactin and heme transport and TonB are required for virulence in the mouse. *Infect. Immun.* **69**, 6179–6185 [CrossRef Medline](#)
 61. Torres, V. J., Pishchany, G., Humayun, M., Schneewind, O., and Skaar, E. P. (2006) *Staphylococcus aureus* IsdB is a hemoglobin receptor required for heme iron utilization. *J. Bacteriol.* **188**, 8421–8429 [CrossRef Medline](#)
 62. Cobessi, D., Celia, H., and Pattus, F. (2005) Crystal structure at high resolution of ferric-pyochelin and its membrane receptor FptA from *Pseudomonas aeruginosa*. *J. Mol. Biol.* **352**, 893–904 [CrossRef Medline](#)
 63. Cobessi, D., Celia, H., Folschweiller, N., Schalk, I. J., Abdallah, M. A., and Pattus, F. (2005) The crystal structure of the pyoverdine outer membrane receptor FpvA from *Pseudomonas aeruginosa* at 3.6 angstroms resolution. *J. Mol. Biol.* **347**, 121–134 [CrossRef Medline](#)
 64. Lukacik, P., Barnard, T. J., Keller, P. W., Chaturvedi, K. S., Seddiki, N., Fairman, J. W., Noinaj, N., Kirby, T. L., Henderson, J. P., Steven, A. C., Hinnebusch, B. J., and Buchanan, S. K. (2012) Structural engineering of a phage lysin that targets Gram-negative pathogens. *Proc. Natl. Acad. Sci. U.S.A.* **109**, 9857–9862 [CrossRef Medline](#)
 65. Payne, M. A., Igo, J. D., Cao, Z., Foster, S. B., Newton, S. M., and Klebba, P. E. (1997) Biphasic binding kinetics between FepA and its ligands. *J. Biol. Chem.* **272**, 21950–21955 [CrossRef Medline](#)
 66. Takeshita, S., Sato, M., Toba, M., Masahashi, W., and Hashimoto-Gotoh, T. (1987) High-copy-number and low-copy-number plasmid vectors for lacZ α -complementation and chloramphenicol- or kanamycin-resistance selection. *Gene* **61**, 63–74 [CrossRef Medline](#)
 67. Klebba, P. E., McIntosh, M. A., and Neilands, J. B. (1982) Kinetics of biosynthesis of iron-regulated membrane proteins in *Escherichia coli*. *J. Bacteriol.* **149**, 880–888 [CrossRef Medline](#)
 68. Neidhardt, F. C., Bloch, P. L., and Smith, D. F. (1974) Culture medium for enterobacteria. *J. Bacteriol.* **119**, 736–747 [CrossRef Medline](#)
 69. Smit, J., Kamio, Y., and Nikaido, H. (1975) Outer membrane of *Salmonella typhimurium*: chemical analysis and freeze-fracture studies with lipopolysaccharide mutants. *J. Bacteriol.* **124**, 942–958 [CrossRef Medline](#)
 70. Hancock, R. E., and Braun, V. (1976) The colicin I receptor of *Escherichia coli* K-12 has a role in enterochelin-mediated iron transport. *FEBS Lett.* **65**, 208–210 [CrossRef Medline](#)
 71. Lugtenberg, B., Meijers, J., Peters, R., van der Hoek, P., and van Alphen, L. (1975) Electrophoretic resolution of the “major outer membrane protein” of *Escherichia coli* K12 into four bands. *FEBS Lett.* **58**, 254–258 [CrossRef Medline](#)
 72. Murphy, C. K., Kalve, V. I., and Klebba, P. E. (1990) Surface topology of the *Escherichia coli* K-12 ferric enterobactin receptor. *J. Bacteriol.* **172**, 2736–2746 [CrossRef Medline](#)
 73. Schneider, C. A., Rasband, W. S., and Eliceiri, K. W. (2012) NIH Image to ImageJ: 25 years of image analysis. *Nat. Methods* **9**, 671–675 [CrossRef Medline](#)
 74. Newton, S. M., Igo, J. D., Scott, D. C., and Klebba, P. E. (1999) Effect of loop deletions on the binding and transport of ferric enterobactin by FepA. *Mol. Microbiol.* **32**, 1153–1165 [CrossRef Medline](#)
 75. Hashimoto-Gotoh, T., Franklin, F. C., Nordheim, A., and Timmis, K. N. (1981) Specific-purpose plasmid cloning vectors. I. Low copy number, temperature-sensitive, mobilization-defective pSC101-derived containment vectors. *Gene* **16**, 227–235 [CrossRef Medline](#)
 76. Hollifield, W. C., Jr., Fiss, E. H., and Neilands, J. B. (1978) Modification of a ferric enterobactin receptor protein from the outer membrane of *Escherichia coli*. *Biochem. Biophys. Res. Commun.* **83**, 739–746 [CrossRef Medline](#)